

The first coordination compounds of OP[NC₄H₈O]₃ phosphoric triamide ligand: Structural study and Hirshfeld surface analysis of Sn^{IV} and Mn^{II} complexes

Mehrdad Pourayoubi, Atekeh Tarahhomi, James a. Golen & Arnold I. Rheingold

To cite this article: Mehrdad Pourayoubi, Atekeh Tarahhomi, James a. Golen & Arnold I. Rheingold (2017): The first coordination compounds of OP[NC₄H₈O]₃ phosphoric triamide ligand: Structural study and Hirshfeld surface analysis of Sn^{IV} and Mn^{II} complexes, Journal of Coordination Chemistry, DOI: [10.1080/00958972.2017.1295139](https://doi.org/10.1080/00958972.2017.1295139)

To link to this article: <http://dx.doi.org/10.1080/00958972.2017.1295139>

 View supplementary material 

 Accepted author version posted online: 13 Feb 2017.

 Submit your article to this journal 

 View related articles 

 View Crossmark data 

Publisher: Taylor & Francis

Journal: *Journal of Coordination Chemistry*

DOI: <http://dx.doi.org/10.1080/00958972.2017.1295139>

The first coordination compounds of OP[NC₄H₈O]₃ phosphoric triamide ligand: Structural study and Hirshfeld surface analysis of Sn^{IV} and Mn^{II} complexes

MEHRDAD POURAYOUBI[†], ATEKEH TARAHHOMI*[‡], JAMES A. GOLEN[§] and
ARNOLD L. RHEINGOLD[§]

[†]Department of Chemistry, Faculty of Sciences, Ferdowsi University of Mashhad, Mashhad 9177948974, Iran

[‡]Department of Chemistry, Semnan University, Semnan 35351-19111, Iran

[§]Department of Chemistry, University of California, San Diego, 9500 Gilman Drive, La Jolla, CA 92093, USA

The first X-ray crystal structures of coordination compounds of OP[NC₄H₈O]₃ phosphoric triamide (*L*) are investigated in Cl₂(CH₃)₂Sn(*trans-L*)₂ (**1**) and [Mn(H₂O)₄(*trans-L*)₂]Cl₂·2H₂O (**2**) as models of molecular and salt complexes for Hirshfeld surface-based analysis. The crystal packing of **1** includes weak interactions, while in the salt complex **2**, a two-dimensional aggregate, along the (001) plane, is mediated by normal O–H...Cl and O–H...O hydrogen bonds. In the Hirshfeld study, the crystal cohesion of **1** and **2** are recognized via H...H, O...H/H...O and Cl...H/H...Cl contacts. Among these interactions, hydrogen bonds O–H...Cl occur in the salt structure of **2**, as well as some weaker hydrogen interactions as C–H...O (**1** and **2**), C–H...Cl (**1**) and O–H...O (**2**). The full fingerprint plots have nearly symmetric shapes for two independent molecules of **1**, while an asymmetric shape appears for the cationic component of **2**. To extract more detailed information on close intermolecular contacts, the molecular surface of the previously reported structure *L* was also mapped. The structure **2** is the first monomeric octahedral Mn(II)-phosphoric triamide complex reported so far. Furthermore, the Hirshfeld surface analysis of **2** is the first such study on a cation-anion complex structure including phosphoric triamide ligand.

Keywords: X-ray crystallography; Phosphoric triamide; Hydrogen bond; Symmetry-independent molecule; Hirshfeld surface analysis

*Corresponding author. Email: tarahhomi.at@semnan.ac.ir

1. Introduction

Phosphoric triamides (PTs) have received attention due to their diverse use as antioxidants [1], Lewis base catalysts [2] and *O*-donor ligands [3-5]. Metal complexes of phosphoramidate ligands have diverse structures and importance of some metal complexes, like organotin(IV)-phosphoramidate complexes, in biological sciences as antifouling, antitumor and antimicrobial agents [6-10]. Mn^{II} has almost not been studied in the phosphoric triamide coordination chemistry, but offers a promising future as there has recently been much interest to the Mn^{II} complexes as polymerization catalysts [11], and also for antibacterial [12] and anticancer [13, 14] activities.

Intermolecular non-covalent interactions such as hydrogen bonds and weak contacts play an important role in assembly of molecules/ions in crystals [15]; so that understanding of such interactions in the crystal structures and controlling of the solid-state behavior of compounds is a noteworthy goal of crystal engineering [16]. Study on such interactions helps to develop procedures for preparation of compounds with desired properties and also to predict the molecular assemblies and structural control of compounds.

Hirshfeld surface (HS) studies offer a resource for visualizing, exploring, analyzing and quantifying intermolecular interactions in crystals with ease, rapidity and immediacy by graphical representations based on three-dimensional HSs and related fingerprint plots (FPs) [17-19]. Although, studying intermolecular interactions may be performed by different methods or software programs, the HS-based method has gained prominence as a valuable graphical tool for clarifying the details of crystalline packing.

Up to now, this method has been used to study intermolecular interactions in a few organotin(IV)-phosphoric triamide complexes [5, 20]. Other metal phosphoric triamide complexes have not been studied with Hirshfeld surface analysis. Study on organotin(IV) complexes are limited to (NHC)(NCC)₂P(O)-Sn and (NHC)₃P(O)-Sn skeletons [5, 20].

In this paper, we present tris(morpholin-4-yl) phosphine oxide (OP[NC₄H₈O]₃ = *L*) in the synthesis of Cl₂Sn(CH₃)₂(*L*)₂ (**1**) and [Mn(H₂O)₄(*L*)₂]Cl₂·2H₂O (**2**), which include six-coordinate Sn^{IV} and Mn^{II} centers. We describe the close intermolecular contacts in the structures, and also for previously reported structure of *L*, using the HS tool with the goal of enabling quantitative comparison between intermolecular interactions in the crystal structures. HS analysis of the

Mn^{II}-phosphoric triamide complex studied here is the first such study on a non-tin metal phosphoric triamide complex.

Based on the knowledge from the Cambridge Structural Database (CSD, version 5.37, Feb. 2016 update [21]), **1** and **2** are the first coordination compounds of OP[NC₄H₈O]₃. One structure of a manganese(II)-phosphoric triamide complex with a Mn–{OP[N(C)(C)]₃}₂ segment has been reported with the commercial ligand hexa-methyl phosphoric triamide (HMPA) (CSD refcode VAYWEY [22]), in which Mn is located in a four-coordinate environment. The structure of **2**, reported here, is the first monomeric octahedral Mn(II)-phosphoric triamide complex.

Apart from HMPA, which were applied in the preparation of 33 organotin(IV) structures [21], no other (NCC)₃P(O)-based phosphoric triamide has been used for preparation of organotin(IV)-phosphoric triamide structures. Due to extensive application of organotin(IV) compounds in biosciences, especially as alternative to anti-cancer cisplatin-based drugs (with high toxicities), this paper introduces a new water-soluble phosphoric triamide ligand which may be useful to extend the organotin chemistry and possible future applications in biochemistry.

2. Experimental

2.1. Materials and measurements

All chemicals were of analytical grade, obtained from commercial sources and used without purification. Infrared (IR) spectra were recorded on a Buck 500 scientific spectrometer using KBr disks. Elemental analyses (C, H and N) were performed using a Thermo Finnigan Flash 1112EA elemental analyzer. Melting points were determined using an Electrothermal IA-9300 apparatus and are uncorrected.

2.2. Syntheses

For preparation of OP[NC₄H₈O]₃, a solution of morpholine in dry acetonitrile was added dropwise to a solution of P(O)Cl₃ in the same solvent (6:1 molar ratio) at 273 K. After stirring for 4 h, the solvent was removed in *vacuo*, and the crude product was used in complexation reactions.

2.2.1. Syntheses of *trans*-dichlorido-*trans*-dimethyl-*trans*-bis[tris(morpholin-4-yl) phosphine oxide-κO]tin(IV), Cl₂Sn(CH₃)₂(OP[NC₄H₈O]₃)₂ (1**).** A solution of Sn(CH₃)₂Cl₂ (1 mmol) in

methanol (5 ml) was added dropwise to an excess of ligand (2.5 mmol) solution in methanol (15 ml). The clear solution was stirred under reflux for 48 h. Colorless crystals were obtained after a few days at room temperature. Yield: 58%. M.p. 205 °C. Anal. Calc. for $C_{26}H_{54}Cl_2N_6O_8P_2Sn$ (830.31): C, 37.61; H, 6.55; N, 10.12. Found: C, 37.70; H, 6.52; N, 10.09. IR (KBr, cm^{-1}): 2966, 2908, 2851, 1654, 1450, 1363, 1299, 1260, 1162, 1114, 1025, 967, 915, 843, 786, 731.

2.2.2. Syntheses of tetraaqua-*trans*-bis[tris(morpholin-4-yl) phosphine oxide- κ O]manganese(II) dichloride dihydrate, $[Mn(H_2O)_4(OP[NC_4H_8O]_3)_2]Cl_2 \cdot 2H_2O$ (2**).** A solution of $MnCl_2 \cdot 4H_2O$ (1 mmol) in methanol/acetonitrile (15 ml; 1:3 v/v) was added dropwise to an excess of ligand (2.5 mmol) solution in methanol (15 ml). The clear solution was stirred under reflux for 48 h. Colorless crystals were obtained after a few days at room temperature. Yield: 52%. M.p. 89 °C. Anal. Calc. for $C_{24}H_{60}Cl_2N_6O_{14}P_2Mn$ (844.56): C, 34.13; H, 7.16; N, 9.95. Found: C, 34.37; H, 7.04; N, 9.98. IR (KBr, cm^{-1}): 3391, 3242, 2968, 2902, 2852, 1654, 1447, 1386, 1301, 1259, 1200, 1106, 1025, 966, 920, 843, 731.

2.3. X-ray measurements

A suitable single crystal for **1** and **2** was selected for X-ray diffraction experiments and mounted on a glass fiber. Details of crystal data and structure refinement have been provided in table 1.

X-ray data for **1** and **2** were collected on a Bruker APEX2 CCD system [23, 24] using Mo $K\alpha$ radiation. Data were corrected for absorption by SADABS [24]. Structures were solved by direct methods, and all non-hydrogen atoms were refined by Fourier full matrix least squares on F^2 . All hydrogens were placed in calculated positions with appropriate riding parameters for **1** and **2**; that is, C–H distances of 0.990 Å for CH_2 and 0.980 Å for CH_3 with 1.20 and 1.50 U_{eq} of parent carbon. For **2**, hydrogens of water bonded to Mn were found from a Fourier difference map and were refined with distance restraints of 0.87 (0.02) Å for O–H and 1.47 (0.02) Å for H...H of H–O–H angle. Hydrogens on solvent waters were not found but were included in chemical formula to obtain correct formula.

In **1**, systematic absences indicated a centrosymmetric space group ($P2_1/c$) and structural solution was refined with two independent molecules in the asymmetric unit with portions of one molecule being disordered. In $Sn1'$, four of the morpholine rings were treated as being disordered

over two positions; that is, for rings N2' and N2A (0.6920/0.3080), for rings N3' and N3A (0.7187/0.2813), for rings N4' and N4A (0.8184/0.1816), and for rings N5' and N5A (0.7652/0.2348). Equal displacement parameter constraints were used for N, O, and C of these rings and distant restraints for P–N of 1.65 (0.02) Å, N–C of 1.47 (0.02) Å, C–C of 1.50 (0.02) Å and C–O of 1.44 (0.02) Å. For this structure, there is also another structural solution provided by SIR97 [25] and some runs of Superflip [26] where the asymmetric unit contains one whole molecule and parts of two molecules with these molecular parts located in special positions. Both structural models, the one with two molecules in the asymmetric unit and the one with one whole molecule and two fractional molecular parts, give similar results. The authors prefer the structure model with two independent molecules because this model is provided by newer versions of SIR as well as most of the Superflip runs.

Structure **2** exhibited chloride and water molecules near symmetry elements and were refined with occupation factors of Cl and O of water at 50% and with the suppression of the generation of special position constraints.

SHELXTL [27], DIAMOND [28] and Mercury [29] programs were used for making the stereo drawings.

2.4. Hirshfeld surface analysis

3D Hirshfeld surfaces (HSs) of **1** and the complex dication of **2** were generated using *CrystalExplorer* 3.1 [30] which accepts a structure input file in CIF format. Bond lengths to hydrogens were set to standard values (C–H = 1.083 Å and O–H = 0.983 Å) during calculations because internal consistency is important when comparing one structure with another. The normalized contact distances d_{norm} based on van der Waals radii [17] were mapped into the HSs (from –0.299 Å to +1.592 Å for **1** and from –0.714 Å to +1.339 for the complex dication of **2**). Close intermolecular interactions identified as red spots on the d_{norm} HSs are listed in table 2. For molecule Sn1' of **1**, the disorder in the morpholine rings was modeled by running the HS analysis for this molecule, beside both possible orientations separately. Then, one orientation of morpholine rings was selected and modeled as fully occupied.

The normalized contact distance d_{norm} is defined based on pair distances d_e , d_i (the distances from a point on the surface to the nearest atom outside and inside the surface, respectively) and van der Waals radii of the atom, given by equation 1.

$$d_{norm} = \frac{d_i - r_i^{vdw}}{r_i^{vdw}} + \frac{d_e - r_e^{vdw}}{r_e^{vdw}} \quad (1)$$

A red-blue-white color scheme is employed for the identification of the regions of particular importance to intermolecular interactions, where intermolecular contacts are shorter or longer or close to van der Waals separations introduced by negative (red color) or positive (blue color) or zero (white color) values of d_{norm} , respectively.

The HS fingerprint plots (FPs) [19, 31] were constructed from the pair distance d_e , d_i for each individual surface spot which quantitatively summarize the information provided by the generated HSs in the two-dimensional grid histograms. The blue-green-red color coding in the FP represents the frequency of occurrence of any given pair of d_i , d_e as low, medium and high frequent occurrence, respectively. For further detailed analysis, the ‘decomposed’ FPs can be used that allow isolation of any given interaction, where only the relevant interactions are colored. These decomposed plots include the reciprocal X...H/H...X contacts in which X is located inside (for X...H/ $d_e < d_i$) or outside (for H...X/ $d_e > d_i$) the generated HS as an H-atom acceptor. The complementary regions, where one molecule is a donor ($d_e > d_i$) and the other as an acceptor ($d_e < d_i$), can be also identified in the FPs [32].

3. Results and discussion

3.1. Structural description

The molecular structures of **1** and **2** are shown in figures 1 and 2, respectively. Selected bond lengths and angles are presented in table 3. For **1**, the asymmetric unit is composed of two symmetry-independent molecules Sn1 and Sn1', while **2** includes one-half of the complex dication, one chloride and one H₂O molecule. In the dication, Mn^{II} is located on an inversion center. Moreover, **2** has chlorides and water molecules disordered through near symmetry elements (figure 2).

In **1** and **2**, the metal has distorted octahedral coordination with two PT ligands *trans* to each other. For **2**, Mn^{II} is also coordinated with four H₂O molecules; the Cl anions are not coordinated. Polyhedra of **1** and **2** are shown in figures 3 and 4.

In both **1** and **2**, the morpholine rings have a chair conformation and P atoms in the ligands have a distorted tetrahedral environment. In **1**, the P=O bond length coordinated to a

metal center is slightly increased in comparison with free OP[NC₄H₈O]₃ (BIVYAG [33]: 1.4891(1) Å), while in **2**, it is slightly decreased (table 3). The P–N bond lengths in both complexes (table 3) do not show significant differences with the values of free OP[NC₄H₈O]₃ (the P–N bond lengths = 1.6375(1) Å, 1.6385(1) Å and 1.7168(2) Å).

The Sn–O, Sn–Cl and Sn–C bond lengths and the Sn–O–P bond angles of **1** are within expected values [9, 18]. There is no analogous monomeric octahedral Mn(II)-phosphoric triamide complex deposited, and the one Mn(II)-phosphoric triamide in the CSD is a four-coordinate complex (VAYWEY [22]). The Mn–O(P) bond length of **2** (2.1103(14) Å) is longer than that in the tetrahedral VAYWEY.

Bond valence sum (BVS) values for tin ions in Sn1 and Sn1' of **1** and for manganese in **2** were calculated as 4.155, 4.224 and 2.192, respectively, which are close to the formal oxidation states of Sn^{IV} and Mn^{II}.

Structure **1** is devoid of strong hydrogen bonds due to lack of appropriate donors and acceptors. In **2**, the O–H units of coordinated H₂O molecules take part in O–H...Cl and O–H...O hydrogen bonds (table 4), which form a two-dimensional layer along the (001) plane (figure 5).

3.2. Analysis of intermolecular interactions by HSs and FPs

3.2.1. HS and FP of L. The d_{norm} HS and decomposed FPs for *L* are displayed in figure 6. The red and pale red spots on HS correspond to the O...H/H...O and H...H contacts (table 2), respectively. The O...H/H...O contacts reflect the C–H...O hydrogen bonds in which the oxygens of NC₄H₈O or P=O are involved.

By inspecting decomposed FPs in figure 6, the highest proportions of interactions are found for H...H contacts which cover a wide range of HS comprising 72.9% marked by the points spread out in the center of FP. These contacts provide the closest interactions, with the minimum $d_i + d_e$ of 2.2 Å. The O...H/H...O contacts are illustrated as points in a relatively large region of d_e, d_i distances ($1.2 \text{ \AA} < d_e, d_i < 2.3 \text{ \AA}$) on the related FP, containing two characteristic spikes approaching (0.9 and 1.2) in the plot, and hence a closest contact near 2.1 Å. For the decomposed H...H FP, the occurrence frequency of H...H contacts is increased in the region of $1.3 \text{ \AA} < d_e, d_i < 1.8 \text{ \AA}$, manifested by color change from blue to green. For the decomposed O...H/H...O FP, such color change is found in small region of $1.4 \text{ \AA} < d_e, d_i < 1.7 \text{ \AA}$.

3.2.2. HSs and FPs of 1. The molecule Sn1' of **1** shows disorder in the morpholine rings; so, the HSs were generated for possible major and minor components in connection with the fully occupied Sn1. In figure 1, the major and minor components are labeled as suffixes "prime" and "capital letter A", respectively. Figures 7 and 8 show the Hirshfeld surface maps of the major disordered component, while the maps in figures 9 and 10 are related to Sn1 interacting with this component. Furthermore, the HSs were generated for the minor component (figures S1 and S2) and Sn1 (figures S3 and S4) separately interacting with each other. By comparing the two models, the proportion of interactions showed changes of less than 0.2%; hence, for the following discussion, the major disordered conformation of Sn1' is treated as fully occupied in connection with the molecule Sn1. The few differences observed in the shapes of FPs (as shown in figures 7-10 and S1-S4) are caused by slightly different distribution of intermolecular interactions.

The vivid red spots on the HSs of molecules Sn1 and Sn1' of **1** in figures 7 and 9 are due to C–H...O hydrogen bonds. These hydrogen bonds arise from interactions between O of the NC₄H₈O rings with the CH of the adjacent NC₄H₈O rings. There are also light red spots on HS which reflect H...H contacts between hydrogens of neighboring NC₄H₈O rings, highlighted by the orange dashed circles in figures 7 and 9. Some of these contacts are also very light or almost white due to the longer H...H distances.

For the HS of Sn1', the most visible color scheme is a large deep red spot (marked by the red arrow in figure 9) formed by the combined C...C and H...H contacts. These contacts which represent the interactions between the same CH₂ groups (H11C–C11'–H11D) of the NC₄H₈O rings in two adjacent Sn1' molecules included one C11'...C11' and two H11C...H11D contacts (table 2).

C–H...Cl hydrogen bonds are also seen on HSs of Sn1 and Sn1' molecules (figures 8 and 10) visualized by very light red spots or almost white areas, in which the hydrogens are related to the NC₄H₈O groups (table 2).

By considering decomposed FPs in figures 7-10, all of them are nearly symmetric relative to the plot diagonal with $d_e = d_i$ values. The molecular interactions in these compounds are predominantly of the H...H type which cover a wide range of HS comprising 71.1% in Sn1 and 71.6% in Sn1'. These H...H contacts marked by the points spread out in the center of the FP provide the closest contacts, with the minimum $d_i + d_e$ value of 2.2 Å. Moreover, the increases of

the occurrence frequencies for H...H contacts are evidenced by color change from blue to green in the regions of $d_e = d_i$ ($\approx 1.2 - 1.7$ Å for both molecules) on the plot diagonal.

The decomposed fingerprint plots of O...H/H...O contacts include 19.8% of total related HS area for both molecules of **1** (figures 7 and 9). These contacts correspond to the C-H...O hydrogen bonds (those described on the related d_{norm} HSs) which are illustrated as the scattered points in the region of the middle, top left and bottom left sections of the plot with minimum $d_i + d_e$ values of 2.4 Å and 2.3 Å for Sn1 and Sn1', respectively. In O...H/H...O FP of Sn1, one very short spike in the bottom left section of the plot (marked by red circle in figure 7) is visible.

The Cl...H and H...Cl contacts combined, represented as characteristic wings at the top left ($d_e > d_i$, H...Cl) and bottom right ($d_e < d_i$, Cl...H) sections of the related plots in figures 8 and 10, comprise 9.1% and 8.6% for Sn1 and Sn1' molecules, respectively.

Finally, visual inspection of FPs in figures 7-10 affirms that although the nature of intermolecular interactions in two independent molecules Sn1 and Sn1' of **1** are similar to each other, there are subtle differences in the distribution of H...H and Cl...H/H...Cl contacts.

Such analyses were only investigated for four organotin(IV)-phosphoric triamide complexes, I to IV in table 5, where a summary of analyses are gathered in a comparison with **1**. As the N-H unit exists in structures I, II and IV, the Cl...H/H...Cl contacts are associated to both intermolecular N-H...Cl and C-H...Cl hydrogen bonds, different from **1** which only includes C-H...Cl interactions. In III, the N-H unit of the C(O)NHP(O) segment takes part in intramolecular N-H...Cl-Sn hydrogen bonds. The N-H units in structures I, II and IV contribute to the contacts manifested (as spikes and red spots). In the absence of N-H in **1**, weak hydrogen bonds show more participation in the contact. For I, II and IV, two sharp spikes correspond to Cl...H/H...Cl contacts with $d_e, d_i > 1.4$ Å; while for III and **1**, spikes are not visible on the related FP due to longer Cl...H distances (for C-H...Cl hydrogen bonds), with $d_e, d_i > 1.6$ Å for III and $d_e, d_i > 1.7$ Å for **1**. The presence of other contacts are related to hydrogen acceptors cooperating in the packing map. For example, in III, the O...H/H...O, F...H/H...F and C...H/H...C contacts are also visible, due to the presence of a free O (non-coordinated), F and unsaturated C as acceptors.

3.2.3. HS and FP of 2. The d_{norm} HS plot of the dication component of **2** and related decomposed FPs are exhibited in figure 11. The O-H...Cl and O-H...O hydrogen bonds in the

crystal structure of **2** (figure 5, tables 2 and 4) can be easily discerned from the HS as large red spots. The C–H...O hydrogen bonds from the interactions between the O atoms and CH groups of the adjacent NC₄H₈O rings (table 2) are visible as light red spots due to the longer H...O distances. No other characteristic contact is seen on the HS.

In figure 11, a visual inspection of decomposed FP for H...H contacts shows that it is approximately symmetric relative to the plot diagonal with $d_e = d_i$ values. FPs with asymmetric shapes are seen for O...H/H...O and Cl...H/H...Cl contacts, where the decomposed FPs show interactions between two different components, [Mn(H₂O)₄(OP[NC₄H₈O]₃)₂]²⁺ with non-coordinated H₂O molecule and Cl⁻. The O...H/H...O and Cl...H/H...Cl contacts are for the non-charged O–H...O and the charged O–H...Cl hydrogen bonds, respectively. The donor OH groups in both cases belong to coordinated H₂O molecules and the acceptor O arises from non-coordinated H₂O molecules. Such asymmetric FPs are expected for structures that contain more than one component (molecule/ion) [34] with interactions between the different species.

As expected, in asymmetric O...H/H...O FP of **2**, the H...O contacts (19.8%) demonstrate a higher proportion than the O...H contacts (10.4%), since the H...O contacts cover the strong O–H...O hydrogen bonds between the OH groups (of [Mn(H₂O)₄(OP[NC₄H₈O]₃)₂]²⁺) and the O (of non-coordinated H₂O) located inside and outside the generated HS, respectively. The O...H contacts correspond to weak C–H...O hydrogen bonds between the CH NC₄H₈O rings with O of the other NC₄H₈O rings. The mentioned H...O contacts are identified as a long broad spike reaching down to near 1.7 Å, providing the minimum $d_i + d_e$ values (figure 11). The O...H contacts encompass the regions of the bottom half (relative to the diagonal plot) of the related FP ($d_e < d_i$) including a very short thin spike reaching down to near 2.4 Å marked by a red dashed circle in figure 11.

The asymmetric Cl...H/H...Cl FP only contains the H...Cl contacts with a proportion of 10.6% (0% for Cl...H contacts) acquired by the presence of uncoordinated chlorides (for H...Cl/ $d_e > d_i$) the generated HS as an H-atom acceptor *versus* the absence of chloride in inside (for Cl...H/ $d_e < d_i$). These H...Cl contacts are points in the regions of the top half of the FP ($d_e > d_i$) relative to the diagonal plot, covering the charged hydrogen bonds O–H...Cl. These regions are narrowed toward points with lower $d_e + d_i$ values as a beak-like spike in the top left corner of the FP.

Similar to **1**, the highest proportions of contacts for **2**, marked by the points spread out in a large area of FP, are observed for H...H contacts (comprising 59.2%). Moreover, the frequency of occurrence of H...H contacts increases in the regions of $d_e = d_i$ ($\approx 1.3 - 1.7 \text{ \AA}$) on the plot diagonal, shown as the bright areas colored from blue to green.

3.2.4. Comparison of HSs and FPs of 1 and 2 with free L. In the absence of any classical hydrogen bond in the structure of *L*, the H...H and O...H/H...O contacts play decisive roles in crystal packing, represented as red spots on the HS, and the O...H/H...O contacts are the weak C-H...O(=P/—C₄H₈N) hydrogen bonds. In HSs of **1** and **2**, O...H/H...O contacts are visible as red spots. Although, the minimum d_e, d_i values of O...H/H...O contacts are slightly enhanced from $d_e = d_i \approx 0.9 \text{ \AA}$ in *L* to $d_e = d_i \approx 1.0 \text{ \AA}$ in **1**. This is due to the non-availability of P=O for hydrogen bond interaction in **1** as it takes part in coordination. In **1**, O of OC₄H₈N takes part in the O...H/H...O contacts, but have lower hydrogen bond acceptor capability with respect to the P=O, reflected in the strength of hydrogen bonds formed. For **2**, the cited minimum d_e, d_i values of H...O contacts in *L* decline to $d_e \approx 0.9 \text{ \AA}/d_i \approx 0.7 \text{ \AA}$ provided by strong O-H...O hydrogen bonds formed. For the O...H contacts, which are related to weak C-H...O hydrogen bonds, the minimum d_e, d_i values from free *L* ($d_e = d_i \approx 0.9 \text{ \AA}$) to complex ($d_e \approx 1.0 \text{ \AA}$ and $d_i \approx 1.4 \text{ \AA}$ in **2**) increase.

The Cl...H/H...Cl contacts, besides the H...H and O...H/H...O, are the other intermolecular contacts in the crystal structures of both **1** and **2** (manifested as light red spots on the related HSs).

In all three structures (**1**, **2** and *L*), the H...H contacts have the most contribution portions, due to the high proportions of hydrogen numbers.

Asymmetry about the plot diagonal is typical of the structures that contain more than one component (molecule/ion). Thus, a symmetric FP is observed for *L* which includes only one complete molecule in the asymmetric unit. For **1**, nearly symmetric FPs are observed for two symmetry independent molecules with the same formula, while for **2** with three different components the FP is completely asymmetric.

4. Conclusion

The OP[NC₄H₈O]₃ (*L*) phosphoric triamide was introduced as a water-soluble ligand and used for preparation of two new coordination compounds. The 3D HSs and associated 2D FPs were applied to expose a detailed investigation of intermolecular interaction networks in the new structures Cl₂(CH₃)₂Sn(*trans-L*)₂ (**1**) and [Mn(H₂O)₄(*trans-L*)₂]Cl₂·2H₂O (**2**) and also in the previously reported structure of free *L*. The manganese(II) complex reported here is the first octahedral Mn(II)–phosphoric triamide with an (NCC)₃P(O) segment. HS analysis is the first such analysis for a non-tin metal phosphoric triamide complex. The obtained results are: (i) The H...H, O...H/H...O and Cl...H/H...Cl contacts play a significant role in the structures of **1** and **2**, shown as red spots on the related HSs. For free *L*, H...H and O...H/H...O contacts (red spots on the HS) contribute considerably to the crystal cohesion. (ii) Full fingerprint of *L* has a symmetric shape, while the full fingerprints of two symmetry-independent molecules of **1** have a nearly symmetric shape. In **2**, the FP has an asymmetric shape as a consequence of the presence of three components in the structure. (iii) A visual evaluation of HSs and FPs simply elucidates a more efficient packing in **2** afforded by the presence of the strong hydrogen bond interactions O–H...O and O–H...Cl in the crystal lattice, where such strong interactions are absent in **1**. (iv) The complexation of *L* with Sn^{IV} in **1** results in reduction of O...H/H...O contacts, due to the involvement of P=O in the Sn–O=P bond and so its non-availability as a H-bond acceptor. Conversely, for **2**, the coordination of *L* to Mn^{II} leads to reduction and increase, respectively, for H...H and O...H/H...O contacts.

Finally, comparison of HSs and FPs of organotin(IV)-phosphoric triamide complex **1** with previously reported analogues, which include only four complexes, reveals that the dominant interactions were the H...H and Cl...H/H...Cl contacts (associated to the N–H...Cl or C–H...Cl hydrogen bonds). The involvement of chloride is due to Sn(CH₃)₂Cl₂ present in the organotin(IV)-phosphoric triamides studied. Additionally, the NH units in the PT ligands, as good H-bond donors, affect the contacts which are predominantly involved in crystal packing.

Supplementary data

CCDC 943564 (**1**) and 943565 (**2**) for the reported complexes contain the supplementary crystallographic data for this paper. These data can be obtained free of charge from the Cambridge Crystallographic Data Centre via www.ccdc.cam.ac.uk/data_request/cif.

References

- [1] S. Dehghanpour, R. Welter, A. Hamady Barry, F. Tabasi. *Spectrochim. Acta, Part A*, **75**, 1236 (2010).
- [2] S.E. Denmark, X. Su, Y. Nishigaichi, D.M. Coe, K-T. Wong, S.B.D. Winter, J. Young Choi. *J. Org. Chem.*, **64**, 1958 (1999).
- [3] A.R. de Aquino, G. Bombieri, P.C. Isolani, G. Vicentini, J. Zukerman-Schpector. *Inorg. Chim. Acta*, **306**, 101 (2000).
- [4] R. Horikoshi, Y. Funasako, T. Yajima, T. Mochida, Y. Kobayashi, H. Kageyama. *Polyhedron*, **50**, 66 (2013).
- [5] M. Pourayoubi, S. Shoghpour Bayraq, A. Tarahhomi, M. Nečas, K. Fejfarová, M. Dušek. *J. Organomet. Chem.*, **751**, 508 (2014).
- [6] A. Matsuno-Yagi, Y. Hatefi. *J. Biol. Chem.*, **268**, 1539 (1993).
- [7] M. Nath, S. Pokharia, R. Yadava. *Coord. Chem. Rev.*, **215**, 99 (2001).
- [8] A. Bacchi, M. Carcelli, P. Pelagatti, G. Pelizzi, M.C. Rodriguez-Arguelles, D. Rogolino, C. Solinas, F. Zani. *J. Inorg. Biochem.*, **99**, 397 (2005).
- [9] A.J. Metta-Magaña, M. Pourayoubi, K.H. Pannell, M. Rostami Chaijan, H. Eshtiagh-Hosseini. *J. Mol. Struct.*, **1014**, 38 (2012).
- [10] M. Pourayoubi, M. Toghraee, R.J. Butcher, V. Divjakovic. *Struct. Chem.*, **24**, 1135 (2013).
- [11] K. Fujisawa, M. Nabika. *Coord. Chem. Rev.*, **257**, 119 (2013).
- [12] P. Dorkov, I. Pantcheva, W. Sheldrick, H. Figge, R. Petrova, M. Mitewa. *J. Inorg. Biochem.*, **102**, 26 (2008).
- [13] D. Zhou, Q. Chen, Y. Qi, H. Fu, Z. Li, K. Zhao, J. Gao. *Inorg. Chem.*, **50**, 6929 (2011).
- [14] X. Chen, L. Tang, Y. Sun, P. Qiu, G. Liang. *J. Inorg. Biochem.*, **104**, 1141 (2010).
- [15] (a) G.R. Desiraju, J.J. Vittal, A. Ramanan, *Crystal Engineering: A Textbook*, p 216, World Scientific, Singapore (2011). (b) D. Braga, L. Brammer, N.R. Champness. *Cryst. Eng. Comm.*, **7**, 1 (2005).
- [16] (a) G. Gilli, F. Bellucci, V. Ferretti, V. Bertolasi. *J. Am. Chem. Soc.*, **111**, 1023 (1989). (b) M.C. Etter, J.C. MacDonald, J. Bernstein. *Acta Crystallogr., Sect. B*, **46**, 256 (1990).
- [17] M.A. Spackman, D. Jayatilaka. *Cryst. Eng. Comm.*, **11**, 19 (2009).

- [18] J.J. McKinnon, M.A. Spackman, A.S. Mitchell. *Acta Crystallogr., Sect. B*, **60**, 627 (2004).
- [19] J.J. McKinnon, D. Jayatilaka, M.A. Spackman. *Chem. Commun.*, 3814 (2007).
- [20] M. Pourayoubi, A. Saneei, M. Dušek, S. Alemi Rostami, A. Crochet, M. Kučeraková. *J. Iran. Chem. Soc.*, **12**, 2093 (2015).
- [21] (a) F.H. Allen. *Acta Crystallogr., Sect. B*, **58**, 380 (2002). (b) C.R. Groom, F.H. Allen. *Angew. Chem. Int. Ed.*, **53**, 662 (2014).
- [22] Z.M. Jin, B. Tu, Y.Q. Li, M.C. Li. *Acta Crystallogr., Sect. E*, **61**, m2510 (2005).
- [23] Bruker, *SAINTE*. Bruker AXS Inc., Madison, Wisconsin, USA (2013).
- [24] Bruker, *APEX2* and *SADABS*. Bruker AXS Inc., Madison, Wisconsin, USA (2014).
- [25] A. Altomare, M.C. Burla, M. Camalli, G.L. Casciarano, C. Giacovazzo, A. Guagliardi, A.G.G. Moliterni, G. Polidori, R. Spagna. *J. Appl. Crystallogr.*, **32**, 115 (1999).
- [26] L. Palatinus, G. Chapuis. *J. Appl. Crystallogr.*, **40**, 786 (2007).
- [27] G.M. Sheldrick. *Acta Crystallogr., Sect. C*, **71**, 3 (2013).
- [28] K. Brandenburg, H. Putz, DIAMOND, Crystal Impact, Bonn, Germany (2005).
- [29] C.F. Macrae, I.J. Bruno, J.A. Chisholm, P.R. Edgington, P. McCabe, E. Pidcock, L. Rodriguez-Monge, R. Taylor, J. van de Streek, P.A. Wood. *J. Appl. Crystallogr.*, **41**, 466 (2008).
- [30] S.K. Wolff, D.J. Grimwood, J.J. McKinnon, M.J. Turner, D. Jayatilaka, M.A. Spackman, *CrystalExplorer 3.1*, University of Western Australia, Crawley, Australia (2013).
- [31] M.A. Spackman, J.J. McKinnon. *Cryst. Eng. Comm.*, **4**, 378 (2002).
- [32] F.P.A. Fabbiani, C.K. Leech, K. Shankland, A. Johnston, P. Fernandes, A.J. Florence, N. Shankland. *Acta Crystallogr., Sect. C*, **63**, o659 (2007).
- [33] C. Romming, J. Songstad. *Acta Chem. Scand. A*, **36**, 665 (1982).
- [34] F.P.A. Fabbiani, J.B. Arlin, G. Buth, B. Dittrich, A.J. Florence, R. Herbst-Irmer, H. Sowa. *Acta Crystallogr., Sect. C*, **67**, o120 (2011).

Figure captions

Figure 1. The asymmetric unit of **1**, showing two independent molecules Sn1 and Sn1' and the atom-labelling scheme for non-C atoms. Displacement ellipsoids are given at 50% probability and hydrogens are drawn as small spheres of arbitrary radii. Disordered oxygens of the major and minor components are labeled as suffixes "prime" and "capital letter A", respectively, and other disordered atoms are not labeled for clarity.

Figure 2. The structure of $[\text{Mn}(\text{H}_2\text{O})_4(\text{trans-OP}[\text{NC}_4\text{H}_8\text{O}]_3)_2]\text{Cl}_2 \cdot 2\text{H}_2\text{O}$ (**2**), showing the atom-labelling scheme for non-C atoms. Displacement ellipsoids are given at 50% probability and hydrogens are drawn as small spheres of arbitrary radii.

Figure 3. Polyhedron view of **1** in the unit cell. Color codes of atoms are: dark green (Sn), light green (Cl), purple (P), red (O), dark grey (C), light grey (H) and blue (N).

Figure 4. Polyhedron view of **2** in the unit cell. Color codes of atoms are: dark green (Mn), light green (Cl), purple (P), red (O), dark grey (C), light grey (H) and blue (N).

Figure 5. Top: Views of crystal packing of **2**, showing a 2D layer generated by O–H...O and O–H...Cl hydrogen bonds (dashed lines, table 4) parallel with the *ab* plane. The Mn^{II} centers and bonds attached to them are highlighted as "ball and stick". Lower: View of O–H...O and O–H...Cl hydrogen bonds (dashed lines) between the complex dication, Cl[−] and H₂O components of **2**.

Figure 6. Top: A view of d_{norm} HS for *L*, surrounded by neighboring molecules associated with close contacts O...H/H...O (black dashed lines) and H...H (orange dashed lines); Lower: Decomposed H...H and O...H/H...O FPs and related percentage contributions to the total HS area for *L*. The full FP appears as a grey shadow below each decomposed plot.

Figure 7. Top: Views of d_{norm} HS for molecule Sn1 of **1**, in two orientations, surrounded by neighboring molecules associated with close contacts O...H/H...O (identified as red spots) and H...H (orange dashed circles); Lower: Decomposed H...H and O...H/H...O FPs and related percentage contributions to the total HS area for Sn1 of **1**. Very short spike on O...H/H...O FP is highlighted by a red circle. The full FP (with values of $1.0 \text{ \AA} < d_e, d_i < 2.7 \text{ \AA}$) appears as a grey shadow below each decomposed plot.

Figure 8. Top: Views of d_{norm} HS for Sn1 of **1**, in two orientations, surrounded by neighboring molecules associated with close contacts Cl...H/H...Cl (black dashed lines); Lower: Decomposed Cl...H/H...Cl FP and related percentage contribution to the total HS area for Sn1 of **1**.

Figure 9. Top: Views of d_{norm} HS for Sn1' of **1**, in two orientations, surrounded by neighboring molecules associated with close contacts O...H/H...O (identified as red spots) and H...H (orange dashed circles). The combined C...C and H...H contacts are marked by a red arrow; Lower: Decomposed H...H and O...H/H...O FPs and related percentage contributions to the

total HS area for Sn1' of **1**. The full FP (with values of $1.0 \text{ \AA} < d_e, d_i < 2.7 \text{ \AA}$) appears as a grey shadow below each decomposed plot.

Figure 10. Top: Views of d_{norm} HS for Sn1' of **1**, in two orientations, surrounded by neighboring molecules associated with close contacts Cl...H/H...Cl (black dashed lines); Lower: Decomposed Cl...H/H...Cl FP and related percentage contribution to the total HS area for Sn1' of **1**.

Figure 11. Top: A view of d_{norm} HS for **2**, surrounded by neighboring components associated with close contacts O...H/H...O (black dashed lines) and H...Cl (orange dashed lines); Lower: Decomposed H...H, O...H/H...O and H...Cl FPs and related percentage contributions to the total HS area for **2**. A red dashed circle on decomposed O...H/H...O FP highlight the very short thin spike. The full FP (with values of $0.9 \text{ \AA} < d_e < 2.5 \text{ \AA}$ and $0.7 \text{ \AA} < d_i < 2.4 \text{ \AA}$) appears as a grey shadow below each decomposed plot.

ACCEPTED MANUSCRIPT

Table 1. Crystal data and structure refinement for **1** and **2**.

	1	2
CCDC number	943564	943565
Empirical formula	C ₂₆ H ₅₄ Cl ₂ N ₆ O ₈ P ₂ Sn	C ₂₄ H ₆₀ Cl ₂ N ₆ O ₁₄ P ₂ Mn
Formula weight	830.28	844.56
Temperature (K)	100(2)	200(2)
Wavelength (Å)	0.71073	0.71073
Crystal system	Monoclinic	Triclinic
Space group	<i>P</i> 2 ₁ / <i>c</i>	<i>P</i> $\bar{1}$
Unit cell dimensions	<i>a</i> = 16.1409(16) Å <i>b</i> = 15.2677(15) Å <i>c</i> = 29.441(3) Å <i>β</i> = 91.794(4)°	<i>a</i> = 8.6360(5) Å <i>b</i> = 9.1771(5) Å <i>c</i> = 14.0202(8) Å <i>α</i> = 85.258(3)° <i>β</i> = 78.430(2)° <i>γ</i> = 63.125(2)°
Volume (Å ³)	7251.7(13)	970.96(10)
<i>Z</i>	8	1
Density (calculated) (g/cm ³)	1.521	1.444
Absorption coefficient (mm ⁻¹)	0.992	0.626
<i>F</i> (000)	3440	447
Crystal size (mm ³)	0.23 × 0.20 × 0.10	0.24 × 0.11 × 0.07
Crystal color / habit	Colorless / flake	Colorless / blade
Theta range for data collection (°)	1.38 to 31.53	2.49 to 27.24
Index ranges	-23 ≤ <i>h</i> ≤ 19 -22 ≤ <i>k</i> ≤ 21 -42 ≤ <i>l</i> ≤ 43	-8 ≤ <i>h</i> ≤ 11 -11 ≤ <i>k</i> ≤ 11 -18 ≤ <i>l</i> ≤ 18
Reflections collected	103240	24205
Independent reflections	22023 [<i>R</i> _{int} = 0.0416]	4304 [<i>R</i> _{int} = 0.0281]
Completeness to theta = 25.00°	99.9%	99.6%
Absorption correction	Multi-scan / sadabs	Multi-scan / sadabs
Max. and min. transmission	0.9073 and 0.8039	0.9575 and 0.8642
Refinement method	Full-matrix least-squares on <i>F</i> ²	Full-matrix least-squares on <i>F</i> ²
Data / restraints / parameters	22023 / 55 / 819	4304 / 6 / 247
Goodness-of-fit on <i>F</i> ²	1.009	1.038
Final <i>R</i> indices [<i>I</i> > 2σ(<i>I</i>)]	<i>R</i> ₁ = 0.0483, <i>wR</i> ₂ = 0.0935	<i>R</i> ₁ = 0.0412, <i>wR</i> ₂ = 0.1096
<i>R</i> indices (all data)	<i>R</i> ₁ = 0.0960, <i>wR</i> ₂ = 0.1138	<i>R</i> ₁ = 0.0476, <i>wR</i> ₂ = 0.1141
Largest diff. peak and hole (e.Å ⁻³)	1.543 and -1.639	1.482 and -1.316

Table 2. The H...X distances [Å] for highlighted interactions in *L*, **1** and **2**.

<i>L</i>					
C12–H12...O2 ⁱ	2.466	C5–H5...O3 ⁱⁱⁱ	2.613	C5–H17...O4 ^{iv} ≡P1	2.283
C1–H13...O3 ⁱⁱⁱ	2.589	C10–H10...O3 ⁱⁱⁱ	2.188	H11...H22 ⁱⁱⁱ	2.267
1					
C16–H16A...O2 ⁱ	2.558	C18–H18B...O3 ⁱⁱⁱ	2.530	C23–H23B...Cl2 ^{vi}	3.011
C1–H1A...O2 ⁱⁱ	2.516	C13 ⁱ –H13D...O6	2.330	C11'...C11'	3.023
C6–H6A...O2 ⁱⁱⁱ	2.646	C21 ⁱ –H21C...O6 ^{iv}	2.408	H11C...H11D	2.177
C1'–H1'B...O5'	2.330	C8–H8A...Cl1 ^v	2.927	H18A...H2'B	2.227
C12 ⁱ –H12C...O5'	2.453	C20–H20A...Cl2 ^v	2.968	H6B...H14D	2.276
C13–H13B...O3 ⁱⁱⁱ	2.482				
2					
O1–H1A...O1W ⁱ	1.786	O3–H3Y...Cl1 ⁱⁱ	2.45	O3–H3Z...Cl2	2.19
O1–H1A...Cl2 ⁱ	2.370	O3–H3Y...Cl1	2.479	O3–H3Z...Cl2 ⁱⁱⁱ	2.417
O1–H1Y...O2W	1.849	O3–H3Y...O2W	2.661	C7–H7A...O6 ^{vi}	2.532
O1–H1Y...Cl1	2.320				

Symmetry transformations used to generate equivalent atoms for *L*: (i): $x - 1, y, z$; (ii): $x + \frac{1}{2}, -y + \frac{1}{2}, z + \frac{1}{2}$; (iii): $-x + 1, -y, -z + 1$; (iv): $-x + \frac{3}{2}, y + \frac{1}{2}, -z + \frac{3}{2}$; for **1**: (i): $-x + 1, y - \frac{1}{2}, -z + \frac{3}{2}$; (ii): $x, -y + \frac{1}{2}, z + \frac{1}{2}$; (iii): $-x + 1, -y, -z + 1$; (iv): $x, -y + \frac{1}{2}, z - \frac{1}{2}$; (v): $-x + 1, -y + 1, -z + 1$; (vi): $-x, -y, -z + 1$; for **2**: (i): $x + 1, y, z$; (ii): $-x + 1, -y, -z$; (iii): $-x, -y + 1, -z$; (iv): $x + 1, y - 1, z$.

Table 3. Selected bond distances (Å) and angles (°) for **1** and **2**.

1			2		
Sn1– C26	2.109(3)	Sn1'– C26'	2.104(3)	Mn1– O1 ⁱ	2.1883(16)
Sn1– C25	2.120(3)	Sn1'– C25'	2.111(3)	Mn1– O2 ⁱ	2.1103(14)
Sn1– O7	2.196(2)	Sn1'– O7'	2.196(2)	Mn1– O3 ⁱ	2.1954(16)
Sn1– O8	2.204(2)	Sn1'– O8'	2.201(2)	P1– O2	1.4789(15)
Sn1– Cl1	2.5579(10)	Sn1'– Cl2'	2.5499(10)	P1– N1	1.6447(18)
Sn1– Cl2	2.5613(10)	Sn1'– Cl1'	2.5518(10)	P1– N2	1.6461(18)
P1– O7	1.490(3)	P1'– O7'	1.494(3)	P1– N3	1.6529(18)
P1– N1	1.632(3)	P1'– N2'	1.556(5)		
P1– N2	1.641(3)	P1'– N1'	1.630(3)		
P1– N3	1.644(3)	P1'– N3'	1.689(4)		
P2– O8	1.492(3)	P2'– O8'	1.488(3)		
P2– N5	1.642(3)	P2'– N5'	1.596(4)		
P2– N4	1.640(3)	P2'– N6'	1.627(3)		
P2– N6	1.644(3)	P2'– N4'	1.665(3)		
O7– Sn1– O8	179.62(11)	O7'– Sn1'– O8'	179.62(12)	O1 ⁱ – Mn1– O1	180.00(8)
O7– Sn1– Cl1	90.99(7)	O7'– Sn1'– Cl2'	91.72(8)	O2 ⁱ – Mn1– O1 ⁱ	91.39(6)
O7– Sn1– Cl2	88.94(7)	O7'– Sn1'– Cl1'	88.20(8)	O2– Mn1– O1 ⁱ	88.61(6)
O8– Sn1– Cl1	88.67(7)	O8'– Sn1'– Cl2'	88.04(7)	O2 ⁱ – Mn1– O3 ⁱ	91.84(6)
O8– Sn1– Cl2	91.40(7)	O8'– Sn1'– Cl1'	92.04(7)	O2– Mn1– O3 ⁱ	88.16(6)
Cl1– Sn1– Cl2	179.59(3)	Cl2'– Sn1'– Cl1'	179.42(4)	O1 ⁱ – Mn1– O3 ⁱ	89.95(7)
P1– O7– Sn1	150.94(15)	P1'– O7'– Sn1'	152.72(17)	O1– Mn1– O3 ⁱ	90.05(7)
P2– O8– Sn1	149.24(16)	P2'– O8'– Sn1'	151.60(16)	P1– O2– Mn1	151.01(10)

Symmetry transformations used to generate equivalent atoms in **2**: (i) $-x+1, -y+1, -z$.

Table 4. Hydrogen bonds for **2** [Å and °].

<i>D</i> - H... <i>A</i>	<i>d</i> (<i>D</i> - H)	<i>d</i> (H... <i>A</i>)	<i>d</i> (<i>D</i> ... <i>A</i>)	∠(<i>DHA</i>)
O1- H1A...O1W ⁱ	0.864(16)	1.786(17)	2.641(5)	170(3)
O1- H1A...Cl2 ⁱ	0.864(16)	2.370(17)	3.189(2)	158(2)
O1- H1Y...O2W	0.874(16)	1.849(19)	2.699(5)	164(3)
O1- H1Y...Cl1	0.874(16)	2.320(16)	3.163(2)	162(3)
O3- H3Y...Cl1 ⁱⁱ	0.843(16)	2.45(2)	3.104(2)	135(2)
O3- H3Y...Cl1	0.843(16)	2.479(18)	3.280(2)	159(3)
O3- H3Y...O2W	0.843(16)	2.661(19)	3.399(5)	147(2)
O3- H3Z...Cl2	0.861(16)	2.19(2)	2.998(2)	156(2)
O3- H3Z...Cl2 ⁱⁱⁱ	0.861(16)	2.417(19)	3.156(2)	144(2)

Symmetry transformations used to generate equivalent atoms: (i) $x+1, y, z$; (ii) $-x+1, -y, -z$; (iii) $-x, -y+1, -z$.

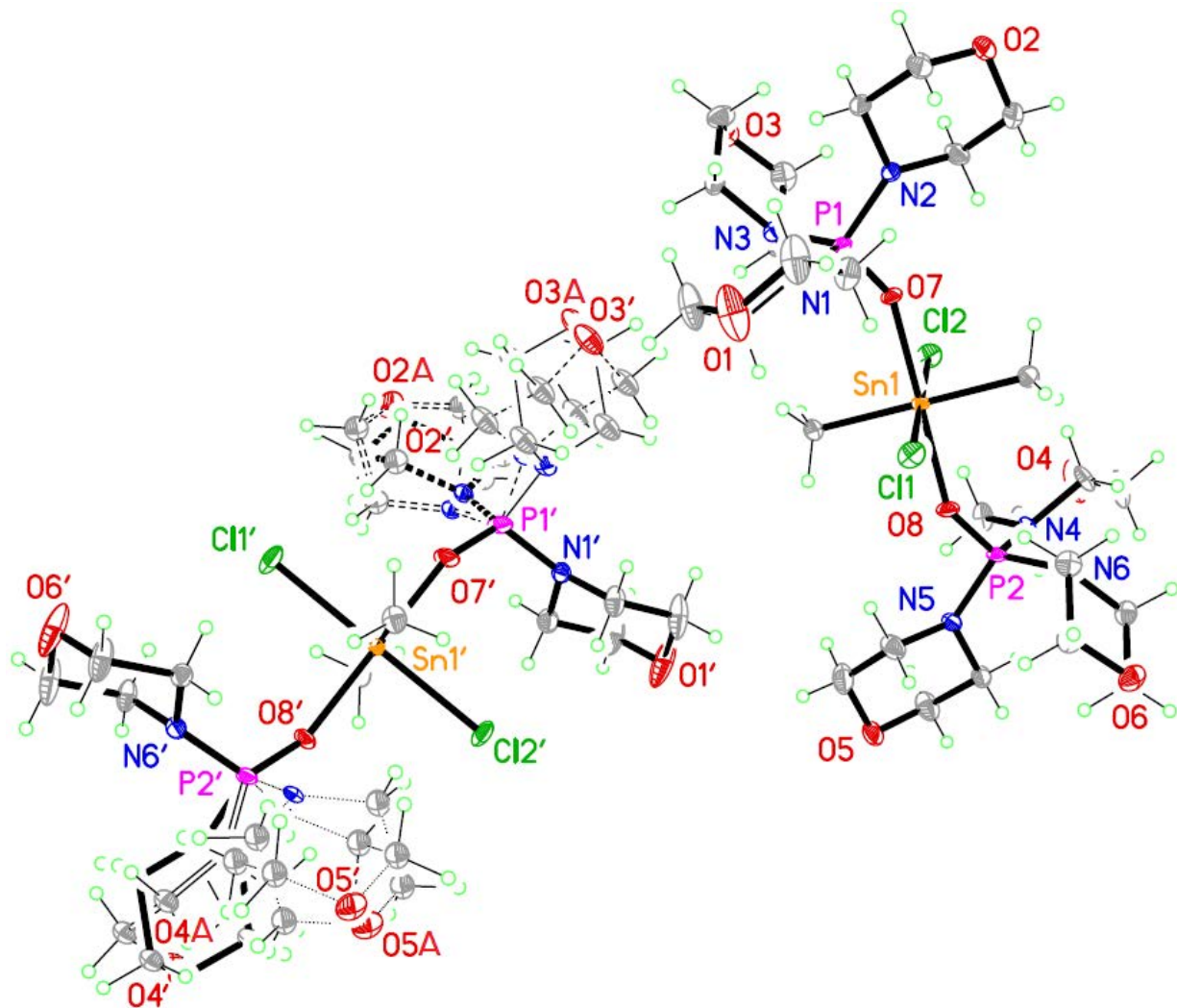
Table 5. Summary of the percentage contributions of interactions for **1**, I, II, III and IV.

	H...H [†]	O...H/H...O	Cl...H/H...Cl	C...H/H...C	F...H/H...F
1	71.1	19.8 (red spot)	9.1	—	—
I [‡]	85.7	0.8	13.1 (red spot)	—	—
II	67.2	—	17.4 (red spot)	—	—
III	68.1	4.6 (red spot)	6.4 (red spot)	11.4	9.3 (red spot)
IV	73.9	—	20.2 (red spot)	5.7	—

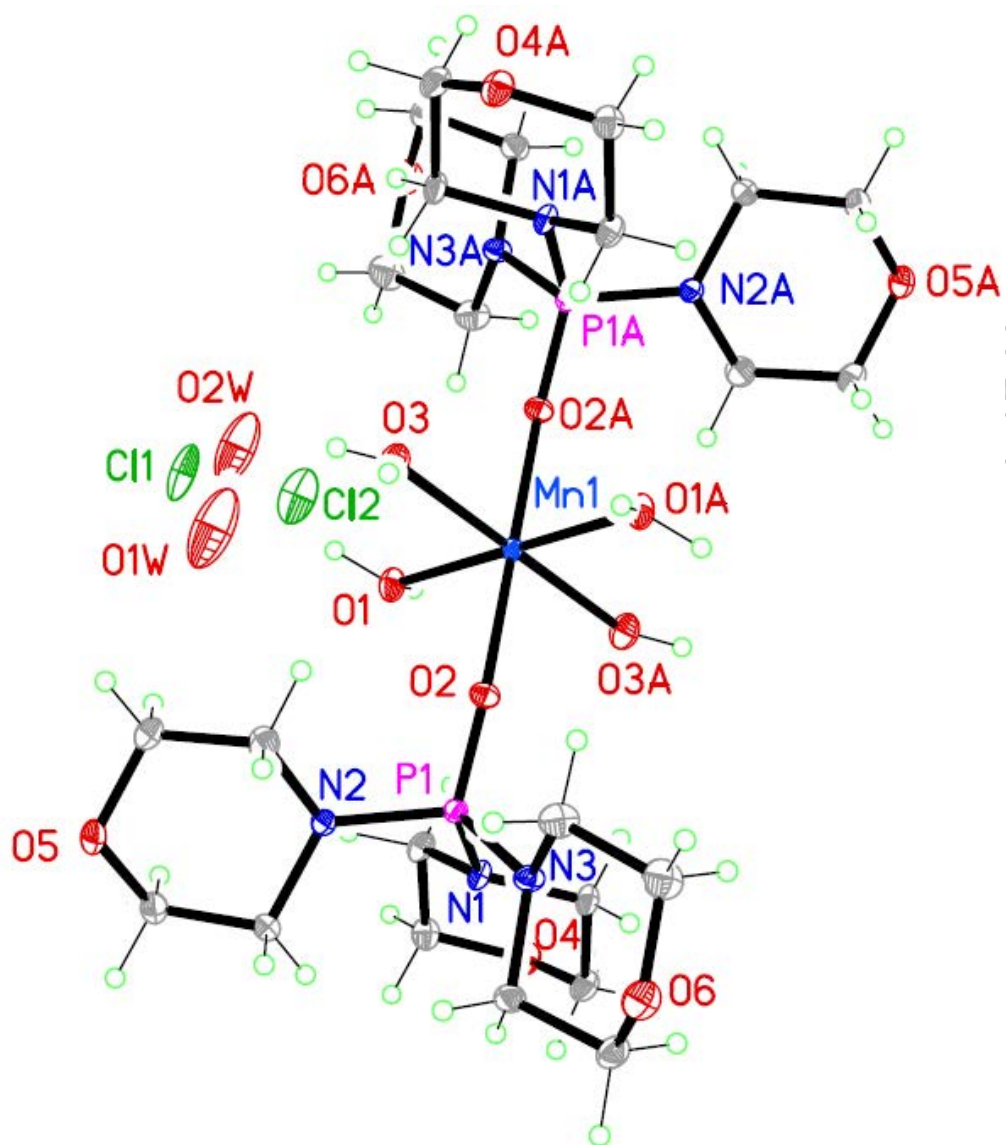
*The formulas of complexes from literature are: $([C_5H_9NH]_3PO)_2SnCl_2Me_2$ (I), $([(CH_3)_3CNH][C_6H_5CH_2N(CH_3)_2PO]SnCl_2Me_2)$ (II), $([3-F-C_6H_4C(O)NH][C_6H_{11}N(CH_3)_2PO]_2SnCl_2Me_2)$ (III) [5] and $([(4-CH_3)C_6H_4NH][C_5H_9(4-CH_3)N]_2PO)SnCl_2Me_2$ (IV) [20].

[†]Some H...H contacts appeared as light red spots on the related HSs.

[‡]Average values of three molecules of I are reported.

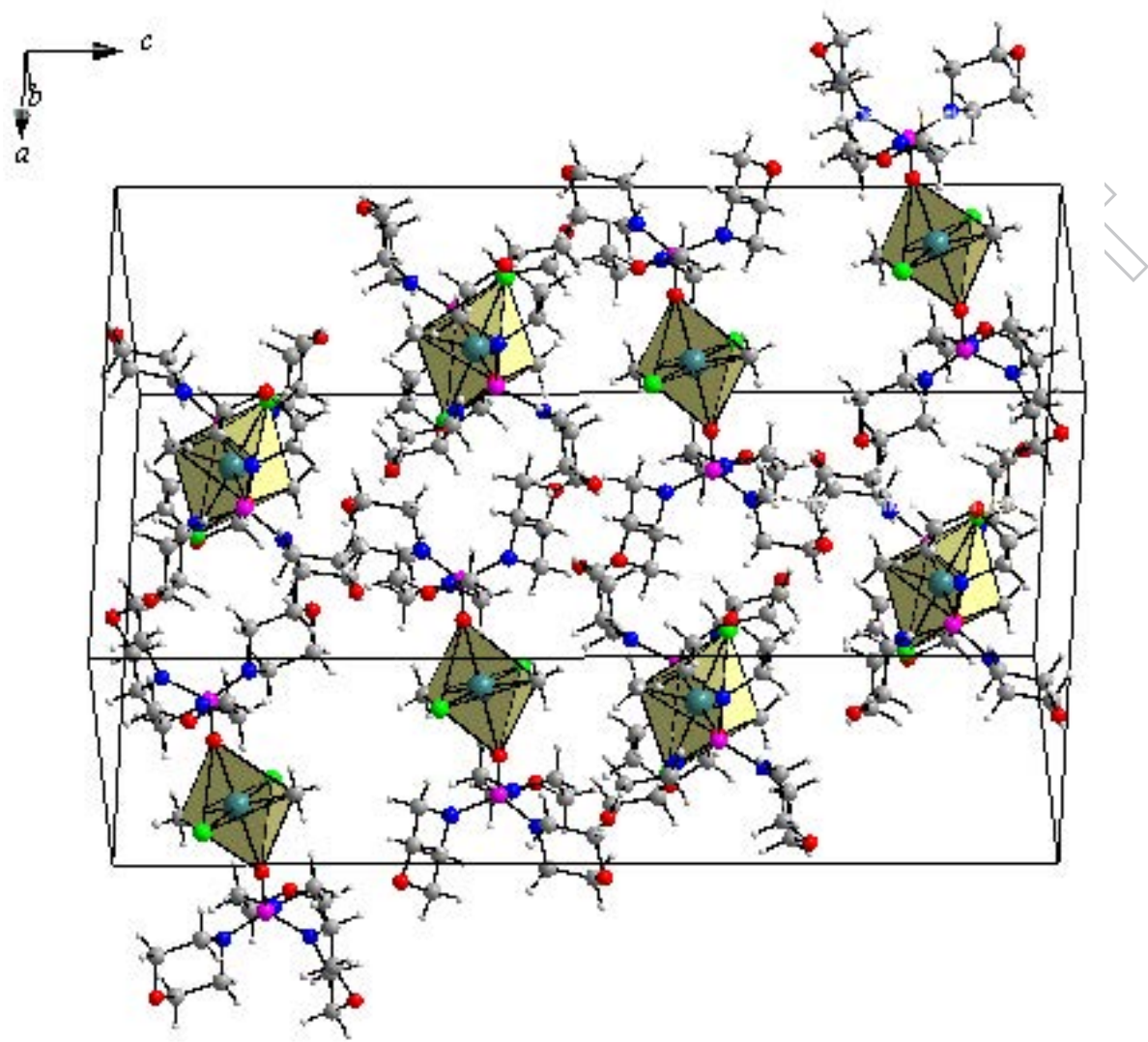


ACCEPTED

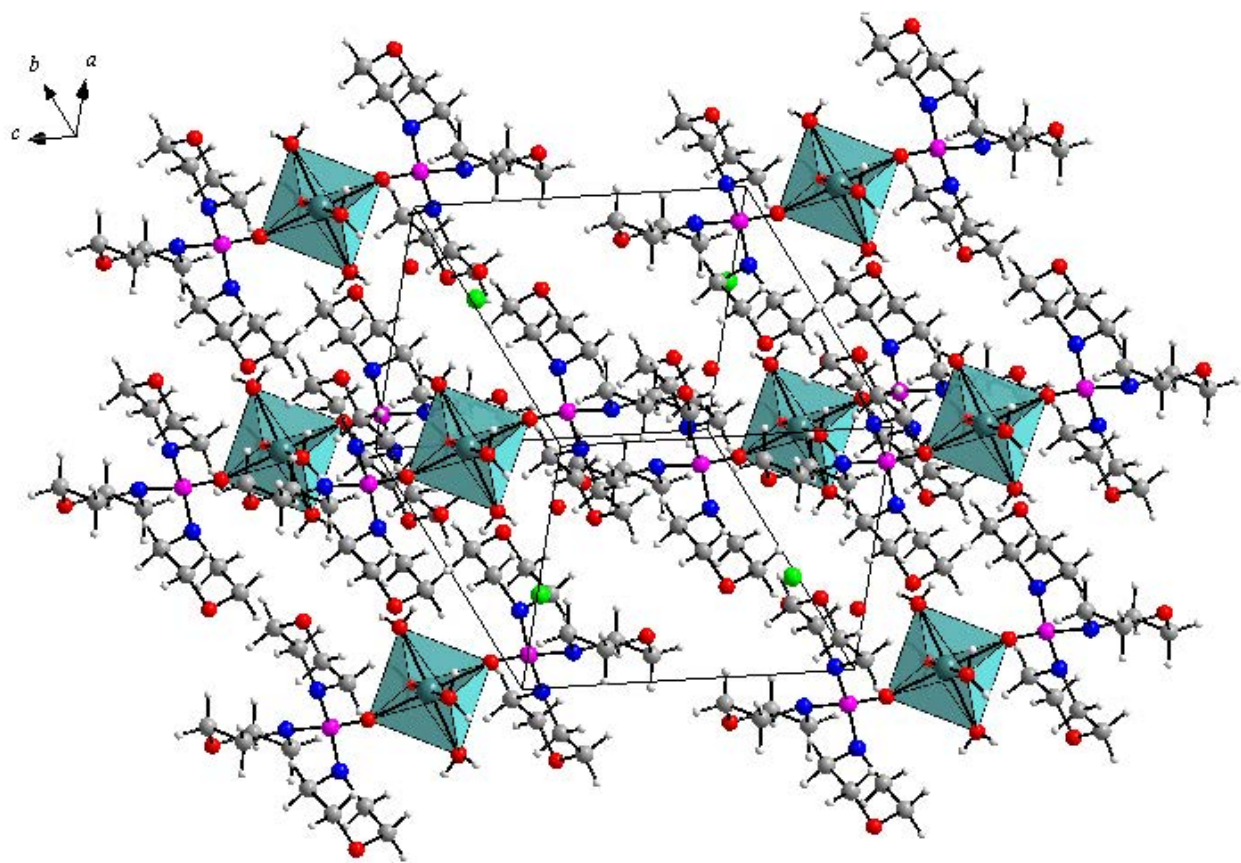


ACCEPTED

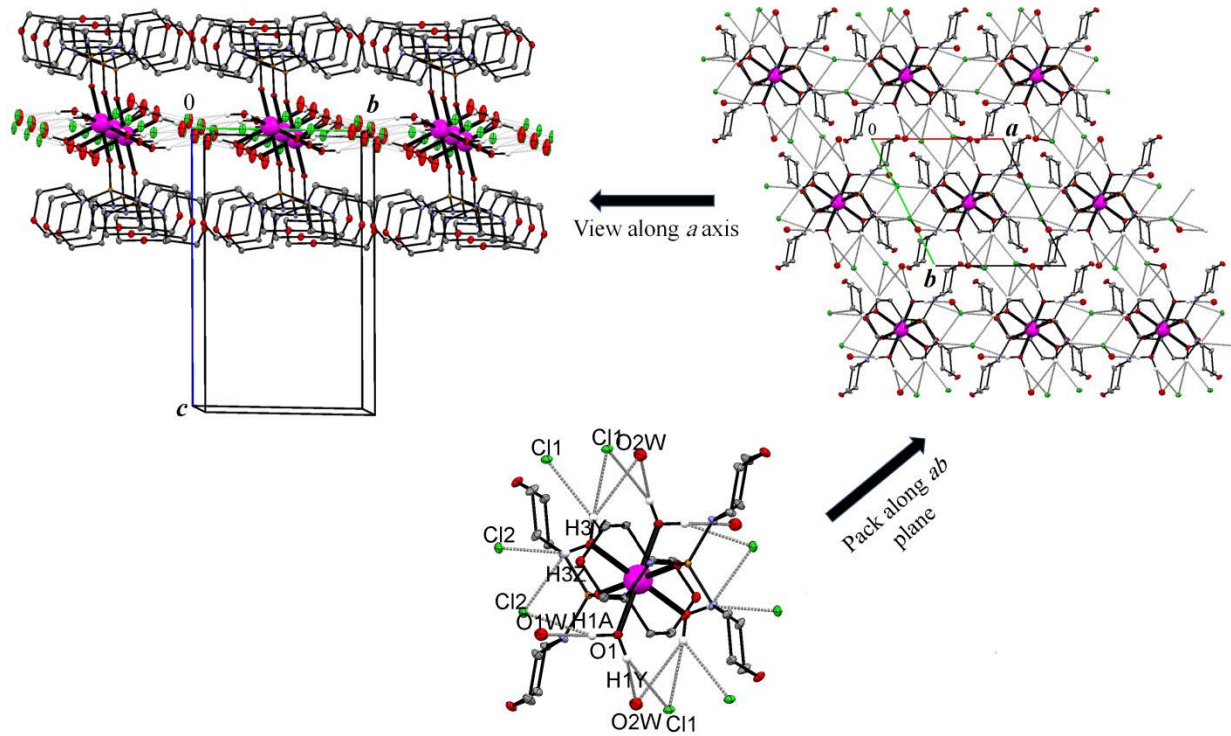
VIPT



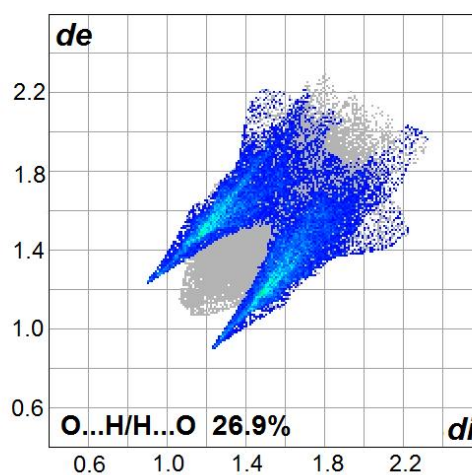
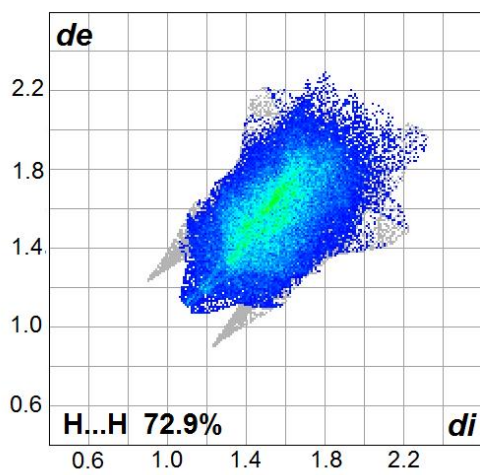
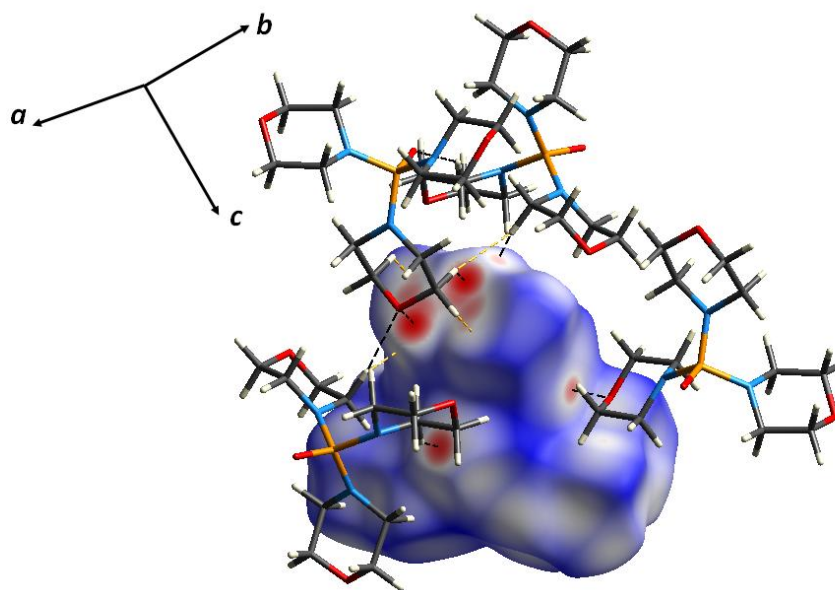
ACCEP



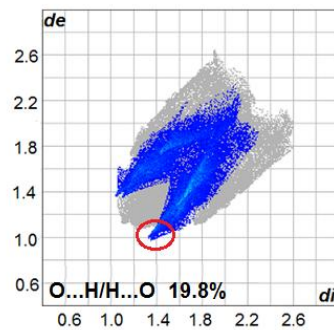
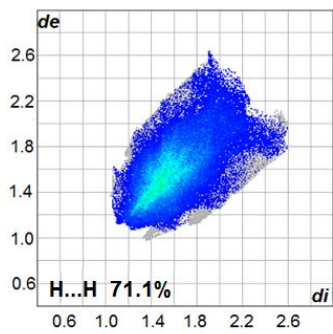
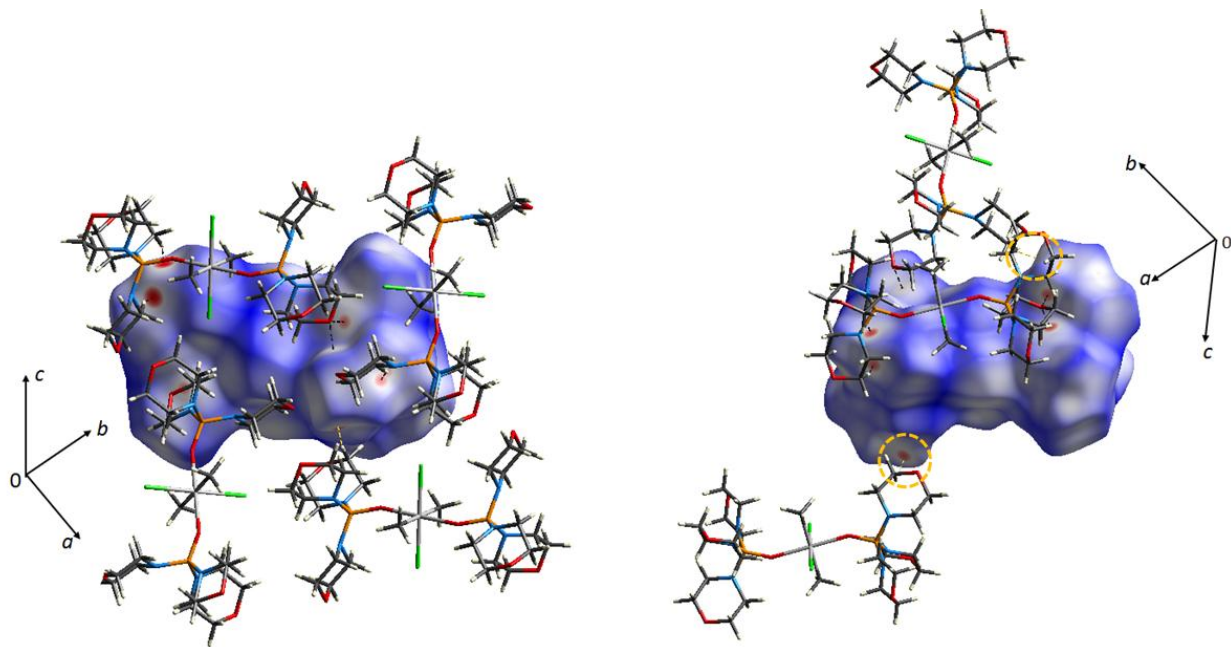
ACCEPTED



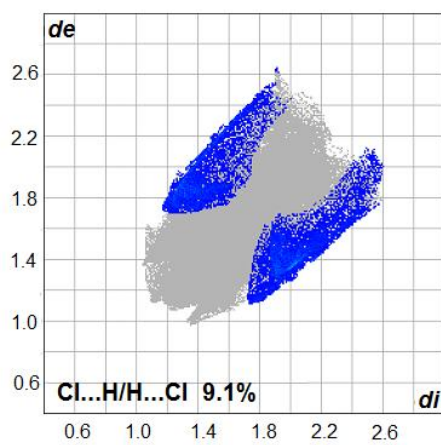
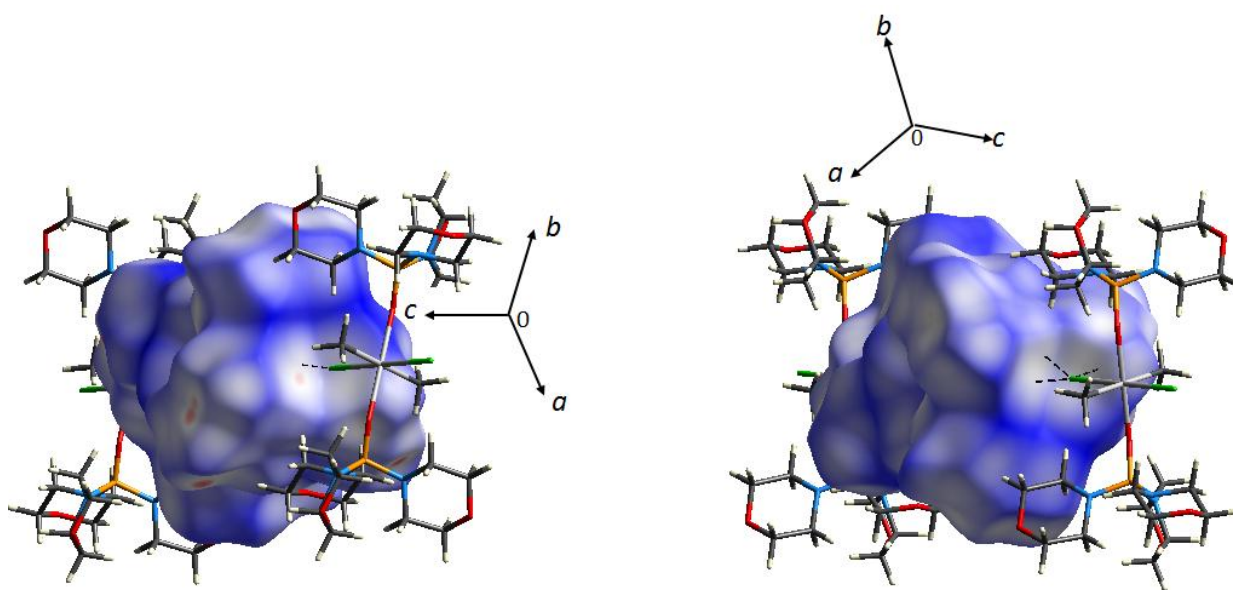
ACCEPTED MANUSCRIPT



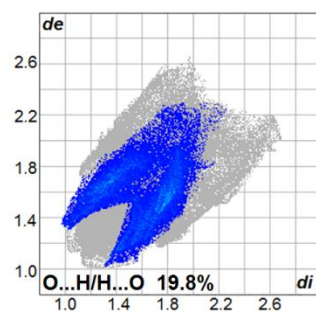
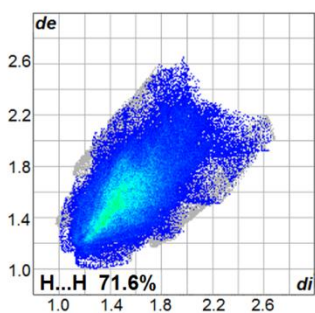
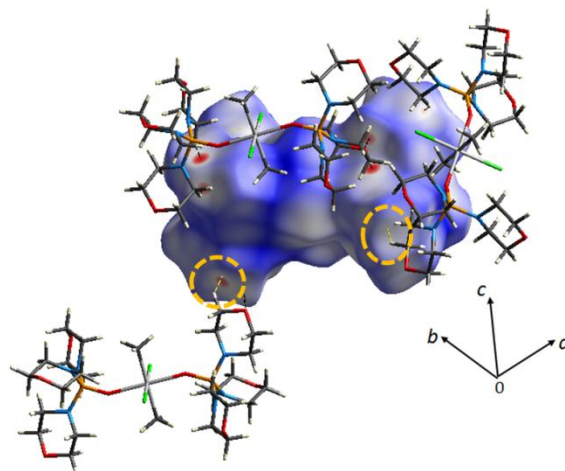
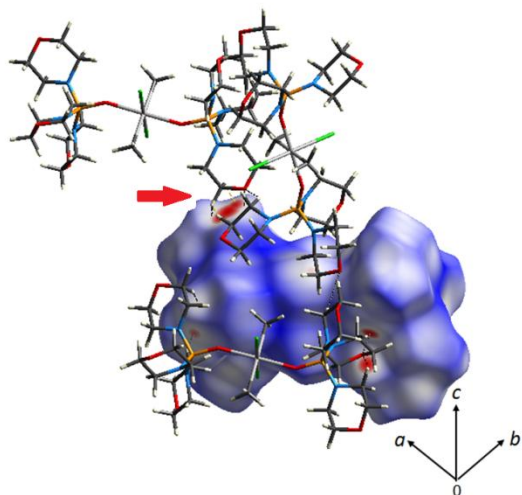
ACCEP



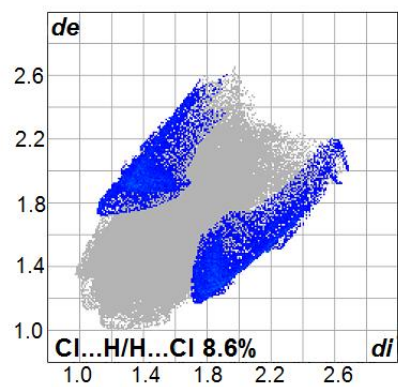
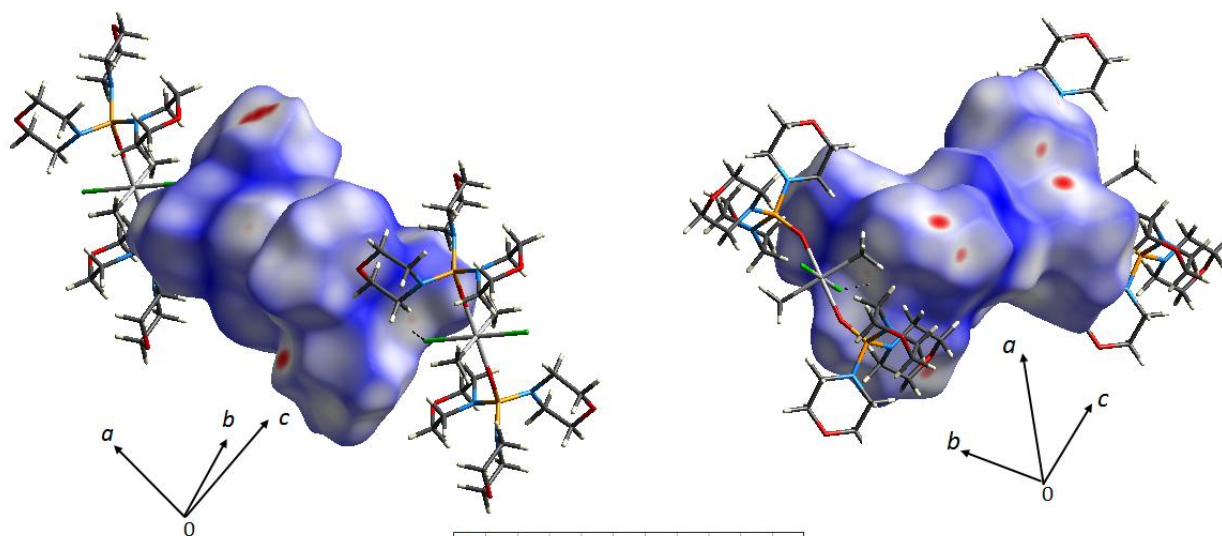
ACCEPTED



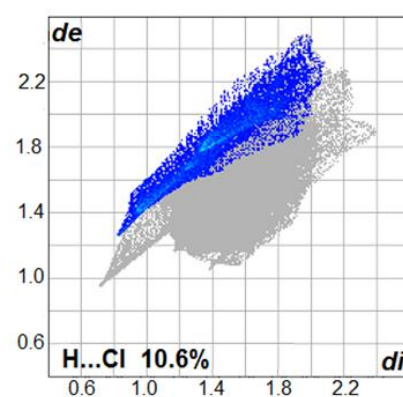
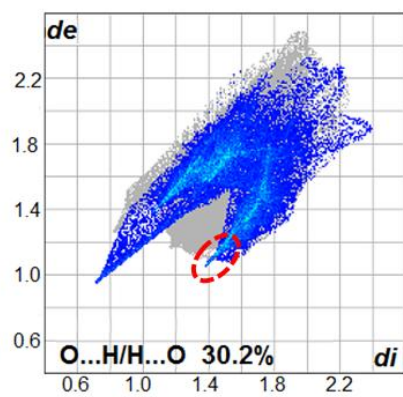
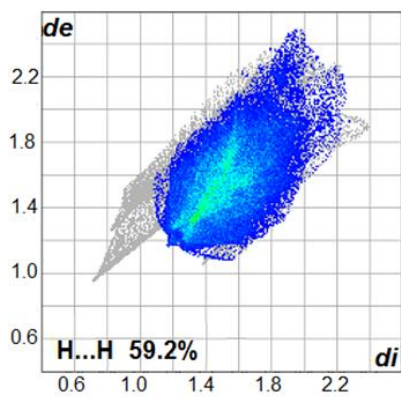
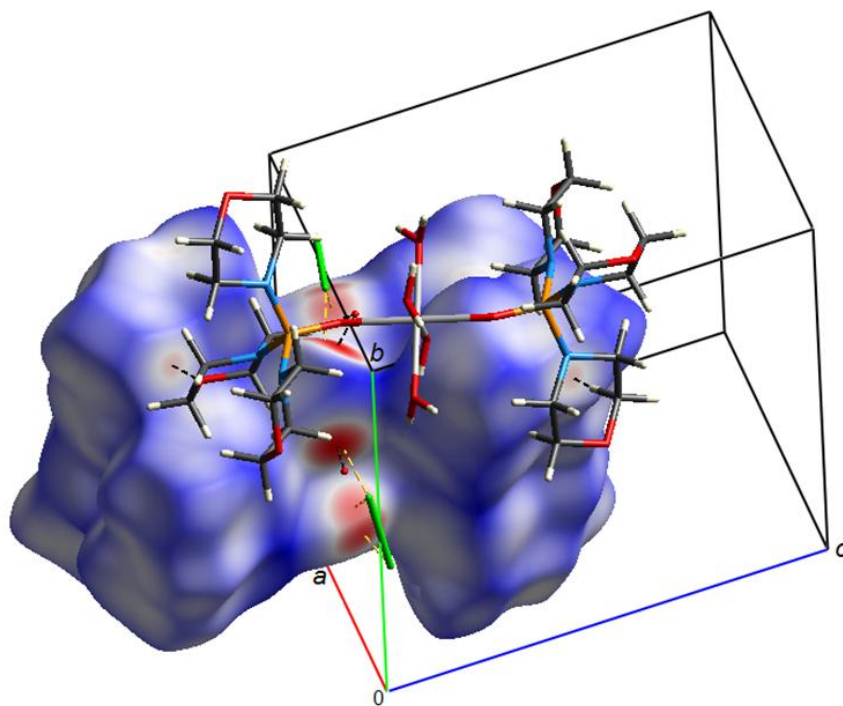
ACCEPTED



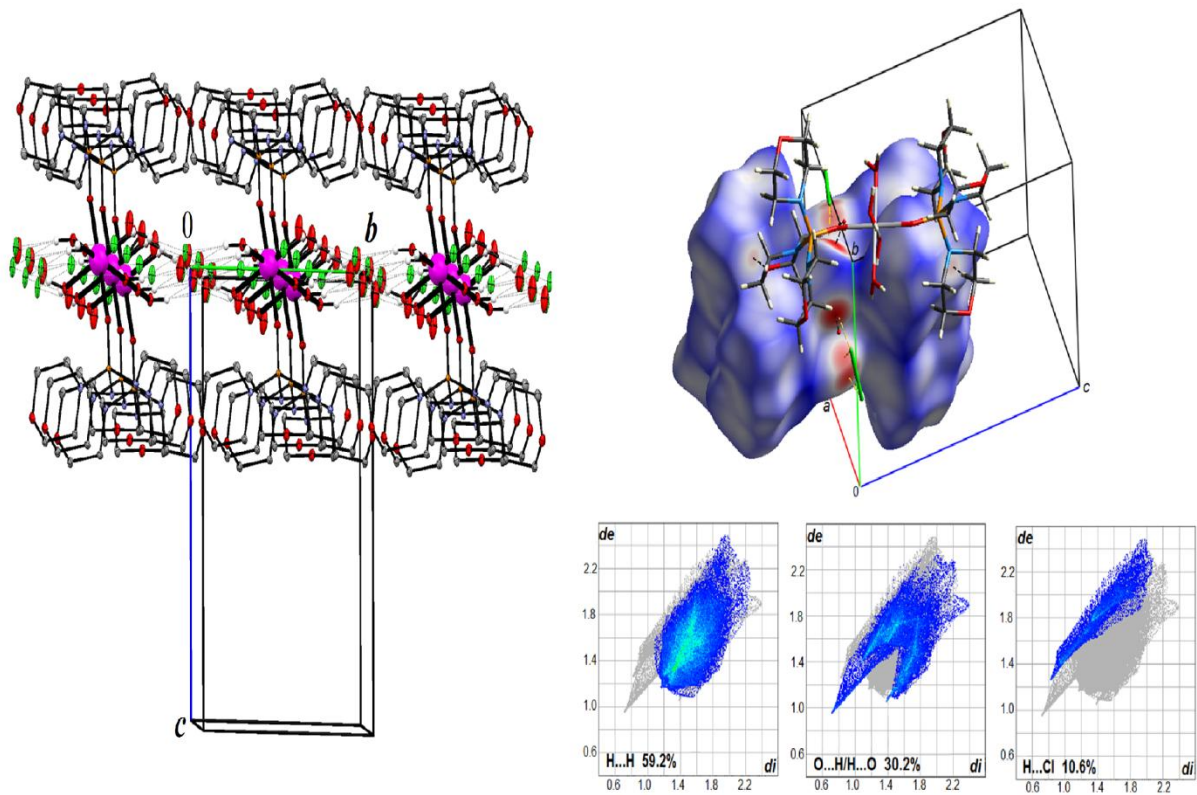
ACCEPTED MANUSCRIPT



ACCEPTED



ACCEPT



ACCEPTED